Journal of Non-Crystalline Solids 358 (2012) 392–398

Contents lists available at SciVerse ScienceDirect

Journal of Non-Crystalline Solids

journal homepage: www.elsevier.com/ locate/ jnoncrysol

Densification modeling of fused silica under nanoindentation

K.R. Gadelrab [a,*], F.A. Bonilla [b], M. Chiesa [a]

[a] Laboratory for Energy and Nano Science (LENS), Masdar Institute of Science and Technology, Abu Dhabi,54224, United Arab Emirates
[b] Asylum Research, Santa Barbara, CA 93117, USA

ARTICLE INFO

Article history:
Received 11 August 2011
Received in revised form 8 October 2011
Available online 8 November 2011

Keywords:
Fused silica;
Elastic modulus;
FEA

ABSTRACT

Fused silica is the reference material used for estimating the area function of nanoindenter tips. Despite being a fundamental step in nanoindentation, little has been done to study its deformation. Under a complex state of stress during indentation, fused silica densifies pointing out that the hydrostatic stress contributes to its yielding. A linear Drucker–Prager model is successfully employed to describe fused silica deformation. Real tip geometry obtained from Atomic Force Microscopy (AFM) is utilized to numerically simulate the area calibration process. Our results indicate a significant discrepancy between the tip area input into our simulation and the one obtained by the calibration process. This implies that the estimated area is not an intensive property of the indenter tip but a convolution of the indenter geometry by the fused silica deformation characteristics and as such may produce erroneous values when used on other materials.

1. Introduction

Nanoindentation is a widely used technique for determining the mechanical properties of materials. The knowledge of the tip area function (the cross sectional area of the tip as a function of the contact depth) is mandatory to be able to calculate the elastic modulus and the hardness of the material. Oliver–Pharr [1] proposed a methodology to determine the tip area function by indenting a reference sample with known elastic modulus and calculate the contact area at different indentation depth. Fused silica is normally chosen as a reference material as it has an isotropic behavior with known elastic modulus of 72 GPa and the material does not show significant pile-up or sink-in during indentation [2]. With the recent applications to nanostructured materials and the increasing trend towards the need for shallow indentations, it is apparent that the calibration process is not sufficiently accurate [3]. Due to the fact that the calibration process sums up all the non-idealities of the indenter tip, it is of limited use to investigate the reasons behind the inaccuracies of the obtained results. Examining the tip geometry and area with other techniques like the Atomic Force Microscope (AFM) has revealed substantial deviations from the area estimated from the calibration process[4, 5].

Although this calibration process is a day to day activity in nanoindentation, we do not really know much about the deformation behavior of fused silica. This is due to the brittle nature of amorphous silica which restricts the characteristic size of the plastic deformation to the micrometer scale [6]. Plasticity in Fused silica cannot be accurately described by the conventional shear flow theories because of two reasons: it is an amorphous material and there is no equivalence to the dislocation based deformation, it has a more open structure than the crystalline materials making it more prone to densification (volume change)[6]. Glass is categorized as “normal” which shows minimal densification and mainly yields by shear flow and “anomalous” which shows significant densification [6–8]. This distinction can be observed in the shape of crack propagation in the Vickers test [8]. Densification was recently studied by Raman microspectroscopy [6, 9, 10] where densification maps and values for the pressure at which fused silica densifies were obtained. It was shown that glass with low Poisson's ratio has an anomalous behavior and fused silica indeed fulfills such condition with a Poisson's ratio of 0.17 [11]. In order to be able to describe correctly the nanoindentation process in fused silica and obtain realistic force curves, one needs to employ an appropriate material model that accounts for the densification behavior.

In this paper, the nanoindentation process on fused silica is modeled using finite element analysis (FEA). For the first time, real tip geometry measured by AFM is utilized to simulate the nanoindentation experiment. The densification behavior of fused silica is described by means of a linear Drucker–Prager model whose parameters are estimated using experimental load indentation curves. The estimated parameters are in agreement with the values published in the literature [7, 12]. The densification maps generated numerically are in excellent agreement with the ones obtained by Raman microspectroscopy underlying that our model correctly describes the yielding behavior of fused silica.

We employ our numerical model to calculate the tip area function as indicated in the ISO 14577. A comparison between the tip area function obtained from the conventional calibration process and the actual tip area function is conducted underlying the great

* Corresponding author. P.O. Box: 54224, Abu Dhabi, United Arab Emirates. Tel.: +971 2 698 8122.
E-mail address: kgadelrab@masdar.ac.ae (K.R. Gadelrab).

0022-3093/$ – see front matter © 2011 Elsevier B.V. All rights reserved.
doi:10.1016/j.jnoncrysol.2011.10.011

discrepancy, in particular at depths under 200 nm, between the real tip geometry and the generated one.

2. Modeling and simulation

Modeling of nanoindentation experiments relies on many assumptions and idealizations concerning the shape of the indenter. Such assumptions range from 2D equivalence of the 3D shape of the tip and angle of the pyramidal shape of the tip to most importantly the tip bluntness [12–19]. Although these assumptions may produce satisfactory results at deep indentations where the tip can be assumed ideal, inaccurate results appear at shallow indentations below 200 nm [3]. This calls for more realistic assumptions.

AFM can be employed to generate accurate 3D scans of the indentation tip. The AFM scans reduce the need for assumptions concerning the shape of the indenter tip and the output from the AFM can be directly used in our modeling.

A Berkovich indenter is scanned using the MFP 3D atomic force microscope. A surface scan in tapping mode, consisting of 512×512 equidistantly distributed scanned points as two dimensional data sets, is performed. In general, the scan size in the x and y direction should be able to capture the overall geometry of the indenter and accurately describe the non-idealities at the apex of the tip. VanLandingham et al. [20] showed that for scan sizes less than 7.5 μm×7.5 μm, the effect of resolution and AFM tip scan speed on the details of the captured image is negligible. Accordingly the scan size in this study is 5 μm×5 μm with scan speed 6.25 μm/s. The procedures mentioned in [5] are followed to avoid the convolution effect of the AFM tip on the Berkovich generated image, namely the sharpness of the AFM tip and the thermal stability of the device during scanning. The tip image generated can be seen in Fig. 1 (a).

We extract the AFM scan in the form of a square matrix having the number of rows and columns equal to the resolution of the scan. The entries of the matrix are the z-heights of every point. A MATLAB script is generated to numerically modify the resolution and the size of the tip scan. This step is necessary to minimize the number of surface elements during the FE simulation. A resolution of 256×256 significantly reduced the number of surface elements used in the simulation while still accurately described the tip geometry. The scan matrix is then transferred into a new form having three columns for the x, y, and z coordinates of every point. This data is used to prepare an Ansys command line to plot the geometrical keypoints of the indenter. An algorithm is then utilized to use triangular areas to connect the keypoints together to generate the surface as shown in Fig. 1 (b).

In such a way we have obtained the real geometrical parameter for the indenter shape with no need for idealized assumptions. The indenter is modeled as a rigid surface. The substrate is modeled as a cylinder with dimensions ($D\times h = 4\times 4.5\ \mu m^2$) which is large enough to avoid the effect of substrate size on the results obtained in the range of indentations performed (max. of 180 nm). Element types and their description are summarized in Table 1. Fine mesh is used near the indentation point to accurately describe the stress around that region. The results obtained are checked against mesh dependency.

3. Material model

Traditional elastic plastic behavior of metals is not suitable for modeling the deformation behavior of fused silica [7, 12, 21]. The hydrostatic component of stress results in densification of the deformed fused silica while experiments show that shear stress also facilitates densification [12, 22, 23]. Accordingly, the yield criterion necessary to model correctly the behavior of fused silica has to account for both effects. Xin and Lambropoulos [12] have proposed a pressure dependent yielding function that resembles the Mohr-Coulomb criteria initially developed for frictional materials [12]. This function used a densification factor α ($0<\alpha<1$) to relate the influence of the hydrostatic to the shear stresses. They utilized FEA to estimate the yield shear stress Y of 9.4 GPa and densification factor α of 0.6 which were able to reproduce the experimental fused silica force curve well. Perriot et al. [6] generated densification maps of fused silica using Raman microspectroscopy below an indentation imprint. The maps show a gradual increase in the densification percent towards 18% close the deformed free surface. Perriot et al. [6] utilized such maps as a method of validation to the numerical results. Comparing both densification maps showed that α significantly affects the numerical maps. With an α of 0.6 the densification map was almost saturated at 16% with a thin region of gradient. It is noted that the densification factor is a weighting factor that is obtained from the fitting process with no clear physical meaning.

Kermouche et al. [7] assumed that such deficiency in the model can be due to the neglection of strain hardening of fused silica. A new elliptical yielding criterion was proposed with a linear hardening function. Kermouche et al. [7] extracted the onset of densification of fused silica by Perriot [24] experiment on diamond-anvil cell DAC to be 11.5 GPa. The numerical force curve obtained from such yield function showed a deviation in the final part of the unloading section when compared to the experimental one. A densification map was generated numerically which showed a remarkable enhancement in the distribution of the densification gradient, but suffered from a saturation of the densification value at 20% close the deformed free surface. To overcome such limitations a different yield function is investigated in the present work.

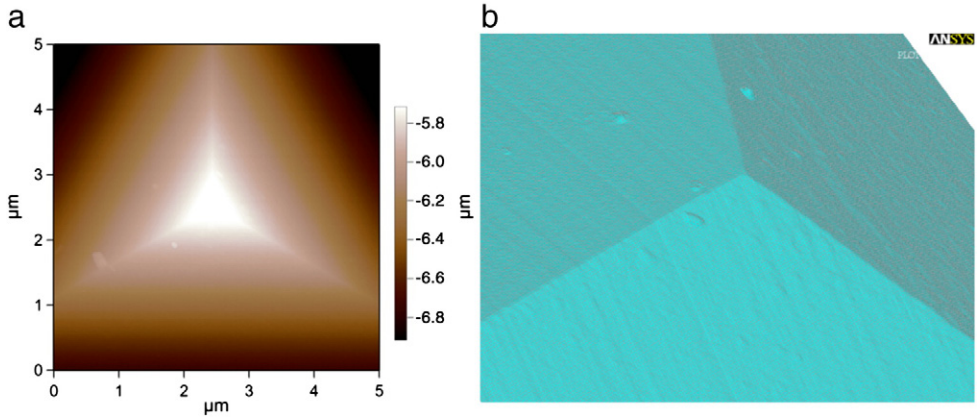

Fig. 1. (a) A Berkovich tip scan obtained at 512×512 scanning resolution with tip speed of 6.25 μm/s. (b) A Surface plot for a Berkovich tip exported from AFM to Ansys with a resolution of 256×256. Triangular areas are used to build the geometry of the tip to generate the whole surface.

Table 1
Description of elements used in FEM and its location.

Element type	Description
SOLID 186	3D solid element for substrate meshing
CONTA 174	Surface element on upper surface of the substrate
TARGE 170	Surface element furnished on the surface of the indenter

The Drucker–Prager model for plasticity in soil and granular materials is one of the most widely used models that account for the influence of the hydrostatic stress component on yielding [25] and as such it is a good candidate to describe the deformation behavior of fused silica. We employ an extended version of the model (extended Drucker–Prager). The extended version accounts for some of the shortcomings of the basic Drucker–Prager model [26]. The linear Drucker–Prager yield function reads:

$$F = q + \beta\sigma_m - \sigma_y = 0, \tag{1}$$

where

$$q = \sqrt{\frac{3}{2} S_{ij} S_{ij}} \tag{2}$$

and $S_{ij} = \sigma_{ij} - \sigma_m \delta_{ij}$ is the deviatoric component of the stress.

$\sigma_m = \frac{1}{3}\sigma_{kk} = -P$, where P is the hydrostatic pressure.

The yield strength under pure shear case is Y. According to von Mises yield criteria

$$Y = \sigma_y / \sqrt{3}. \tag{3}$$

The yield function describes the yield surface in stress space. The normal can be expressed as

$$\mu_{ij} = \frac{\partial F}{\partial \sigma_{ij}} = \beta \frac{\delta_{ij}}{3} + \frac{3 S_{ij}}{2q}. \tag{4}$$

When the inner product $\mu_{ij}\, d\sigma_{ij} > 0$, this indicates material loading, while the opposite indicates that material is unloaded. Associated plasticity is considered in this analysis.

In the linear yield function for Drucker–Prager, (1), the coefficient β can be considered as follows. In case of pure shear loading $\sigma_m = 0$ and accordingly at yielding $q = \sigma_y$. This is the well known yielding criteria of von Mises. In case of pure hydrostatic stress loading $q = 0$, $\sigma_m = -P$ and $\beta = -\sigma_y / P$ where P will be the pressure at which the material yields in pure hydrostatic loading, so β is considered to be the ratio between the yield strength of the material to the yield stress in pure hydrostatic loading. The fitting process becomes easier as only two parameters are estimated. It is noted that this model does not account for time dependent properties of material like creep or stress relaxation. The success of the constitutive model in reproducing the densification behavior of fused silica is discussed in the following.

4. Experimental procedures

A fused silica sample is indented by means of a Berkovich tip under force control mode. An AFM scan of the sample surface estimated the surface roughness to have an RMS of 1.7 nm. This is considered smooth enough to not affect our indentation results in our range of penetration [27]. The Berkovich tip is made of industrial diamond with Elastic modulus of 865 GPa and Poisson's ratio of 0.2. The indentation process is performed with an MFP Nanoindenter. In order to obtain the highest quality raw data, the acoustic enclosure for the instrument is furnished with a temperature control unit to avoid any thermal drifting during the experiments. This condition, negligible thermal drift in the three axes X, Y, and Z, is verified experimentally. The indenter is pushed to reach a force of 1.25 mN after which it dwells for 10 s. The indenter is then retracted back under the same force (stress) rate used in loading. Three sets of experiments are performed to calibrate the model.

5. Results

Experimental force indentation curves include both loading and unloading cycles. The loading cycle describes the elasto-plastic behavior of the material while the unloading cycle is elastic [3, 4, 28]. Accordingly, the elastic unloading curve is used to estimate the elastic modulus of fused silica by matching the slope of the experimental force curves with the slopes of the simulated force curves while keeping the plastic properties constant. The force-displacement curve of a material with larger elastic modulus yields a higher maximum force value and a different slope in the unloading section. The higher force is due to the deformation of the elastic matrix surrounding the plastified zone under the indenter tip [29].

After determining the elastic modulus of fused silica, the plastic properties of fused silica in (1) is estimated by fitting the loading section of the experimental force indentation curve. The results of the fitting are summarized in Table 2. Fig. 2 shows the resulting force curve from the fitting process. The numerical solution shows very good agreement with the experimental data.

To check the validity of the proposed linear Drucker–Prager model to describe the densification of fused silica, a 2D simulation for the indentation process is performed with an equivalent conical indenter for a Vickers tip. Fig. 3 shows a comparison between our numerical densification results and the experimental results obtained from Raman Microspectroscopy [6, 7]. The densification results are in excellent agreement with the experimental ones, with maximum densification found under the tip. The FEA shows concentric contours of equal density zones while the distribution deviates from the experimental one at the outmost zone. The experimental map shows an extension of the low densified area towards the free surface. This can be attributed to the axis symmetry assumption in modeling the Vickers indenter where the effect of the edges of the Vickers indenter is not taken into account.

The numerical solution in Fig. 3 showed a very interesting distribution of the densification map. The material under the densified zone shows a slight expansion by less than 3%. Although this was not examined experimentally, one can relate this to the elastic properties of the material which tried to expand back after load removal producing these tensile stresses and volume expansion.

At this point, it is important to address the differences in modeling fused silica as an elastic perfect plastic material with respect to the proposed constitutive model. A densification simulation utilized the previously obtained plastic properties in Table 2, while the value of the reduced modulus utilized equals 68 GPa. The elastic perfect plastic analysis used the same reduced elastic modulus of 68 GPa and a yield strength of 6 GPa. The value of the yield strength is obtained by trial and error till the obtained force curve is almost identical to the one obtained by densification as seen in Fig. 5. This value is close to the one used by Shim et al. [17] which was 5.5 GPa. It is interesting to see that although the elastic modulus is kept constant, the curves can be easily distinguished at the lower 30% of the unloading curve. Fitting mid 80% of unloading curves with the Oliver Pharr

Table 2
Summary of the values of fused silica resulted from fitting the experimental force curves.

Elastic Modulus (E)	Yield strength at pure shear (Y)	Yield strength at pure hydrostatic (P)
70.2 GPa	6.35 GPa	11.5 GPa

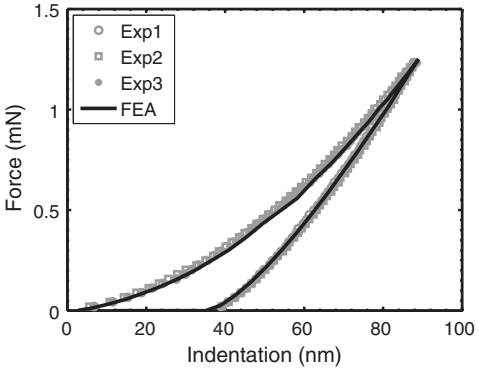

Fig. 2. Calibration of the numerical model with load indentation curves of three experiment sets. Very good agreement is observed between the model and the experiments.

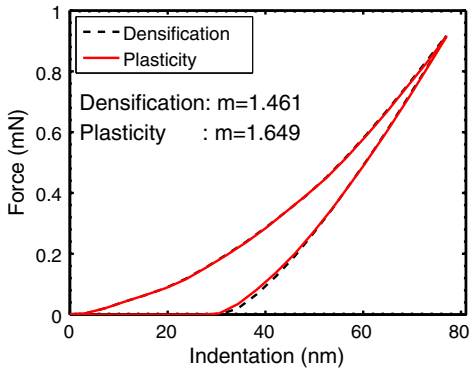

Fig. 4. Numerical force curves obtained by Drucker–Prager model and elastic perfect plastic model. The two curves are almost identical except at the lowest portion of the unloading curve. Fitting the mid 80% of the unloading curve results in two significantly different powers (m) of Oliver Pharr power function.

power function [1] resulted in a significantly different powers m for the power law function as shown in the figure. On the other hand, fitting the upper 50% of the curve resulted in very close values of m for the two simulations (Fig. 4).

To get a better idea behind the reason for the discrepancy in the unloading curve near the end of the unloading, the stresses in the deformed region and its shape are examined. Fig. 5 shows the Von Mises stress distribution in the deformed region after unloading for (a) perfect plasticity yielding and (b) Extended Drucker Prager yielding. The plasticity yielding results in a very localized deformation under the tip edges that decays fast towards the tip faces. On the other hand, The Extended Drucker Prager yielding shows a higher value of residual stresses that extends away from the edges to the surface.

A section through an edge and an adjacent face is obtained for the deformed surface after unloading as shown in Fig. 6. It is worth noting that the term edge becomes trivial in this kind of simulations as there are no sharp edges or reference geometries for the indenter in contrast to the idealized case, however, the two sections of the deformed surfaces in the two models are exactly at the same location.

The deformed surfaces are significantly different. The densification model generates a deeper indent with narrow geometry in contrast to the perfect plasticity model. This means that the elastic recovery from densification pushes the free surfaces of the imprint and tends to narrow it. It is also noted that the densification model resulted in material pile up to about 3 nm at the face of the tip and this is missing in the case of perfect plasticity. This can be related to the stress distribution plot that shows that the material under the tip face demonstrates a high stress value. Experimentally, fused silica pile up has been observed in AFM scans of the remaining indent as seen in Fig. 6 with a pile up value very close to the simulation. Furthermore, Howell et al. [30] has conducted a study on pile up in reference glass and showed that fused silica shows small pile up in the same load range used in our numerical study, in comparison to other types of reference glass [30]. This is one of the main reasons that made it a common calibration material for tip area function. The above indicates that the densification model is better suited for the numerical investigation of the calibration process.

6. Discussion

The Drucker Prager model was shown to reproduce the experimental force curve in a very satisfactory way. It also generated a densification map that is a close match to the one generated by Raman microspectroscopy. In contrary to the model proposed by Xin and Lambropoulos [12], it does not have a floating parameter α that is employed to fit the data without a clear physical meaning. Furthermore, the Drucker Prager yield function has an inherent isotropic strain hardening behavior meaning that the overall yield strength of the system increases in case of having a compressive hydrostatic component of stress. This is probably why the value for Y is in close agreement to the value obtained by the strain hardening model proposed by Kermouche et al.[7] , but with a better agreement to the experimental results. Being able to model fused silica deformation, we can address the problem of tip area function calibration in nanoindentation experiments.

Determining the tip area function is crucial to calculate the elastic modulus of the indented material [1, 20, 31]. ISO 14577-4 describes different methods to calibrate the tip area function where each method has assumptions related to the variation of the properties of the indented reference material with depth and previous knowledge of frame compliance. However, Herrmann et al. [31] used method 4 (ISO 14577-4) and showed that the values of the frame compliance and the tip area function are related where an error in estimating

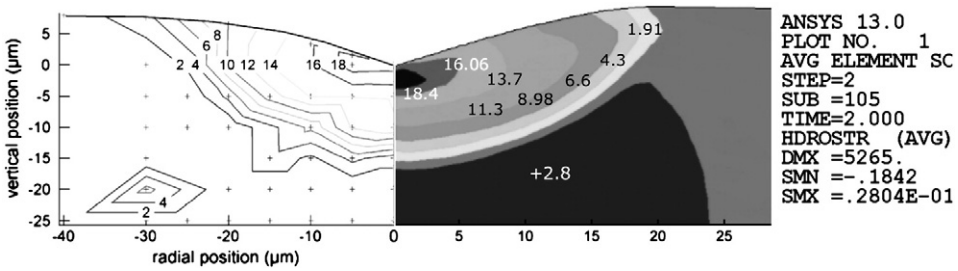

Fig. 3. Comparison between the numerical densification maps in percentages (on the right side) and the experimental results obtained from Raman Microspectroscopy (on the left side)[6, 7]. The +2.8% is an expansion in underlying material. This can be attributed to the elastic recovery of the material after load removal.

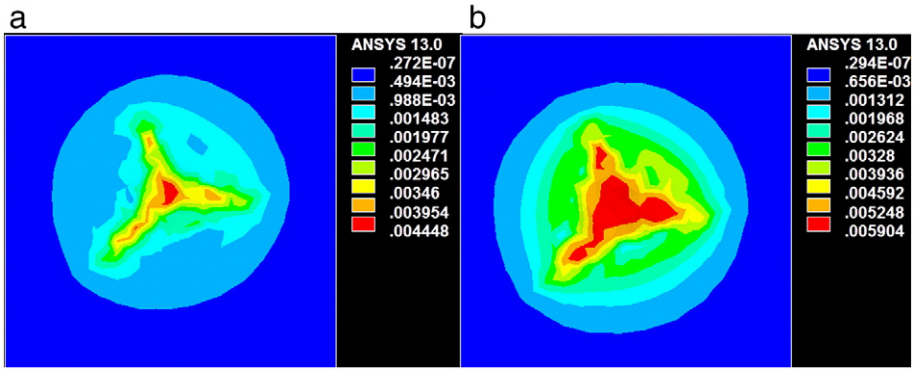

Fig. 5. Von Mises stress distribution after unloading. (a) Elastic perfect plastic (b) Extended Drucker Prager. The residual stresses are higher in the case of Drucker–Prager model that extends away from the edges. Perfect plasticity shows a very localized yielding under the edges of the tip.

one of them will produce a wrong value in the other. The uncertainty becomes even more pronounced using the iterative method of Oliver Pharr [31]. Consequently, efforts have been raised to propose a material independent calibration method utilizing tip metrology from AFM [31–34].

VanLandingham et al. [20] compared the AFM tip area function with the one obtained from fused silica calibration where the AFM scan generated an area higher than the one obtained from fused silica. On the other hand, Meneve et al. [32] showed that the AFM area function generated was lower than the one obtained on fused silica and it depends on the value of the frame compliance used in the iterative process. Lately, Chudoba and Jennette [4] derived a correction factor based on the radial displacement outside the contact region, but the analysis resulted in an area function smaller than the one obtained from the AFM in the first 300 nm. This was justified by not taking into account the densification of fused silica and the simple conical geometry utilized to derive the model [4]. Fig. 7 shows a typical experimental tip area function curve of a Berkovich tip obtained by indenting fused silica employing Oliver Pharr power function [1] (OP func.) and a quadratic fitting function (QD func.) with no correction factors and elastic modulus obtained in Table 2. The contact depth h_c is evaluated with an ε of 0.75. The material dependent method significantly overestimates the area function. This agrees with the observation presented by Troyon and Huang [35] when they were referring their experimental area function to the ideal Berkovich shape and they showed an over estimation of 26% that can't be explained by the correction factors proposed in the literature [2, 36, 37].

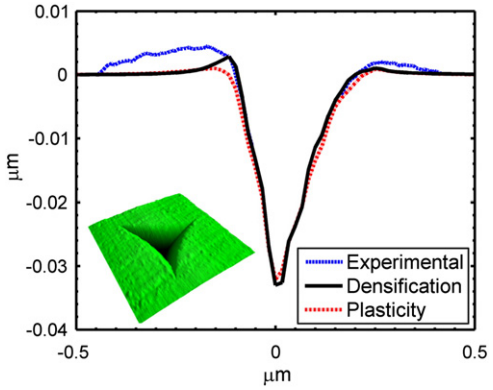

Fig. 6. Indent profiles obtained numerically for Drucker–Prager model and elastic perfect plastic model. The densification model produces a narrower and deeper indent than the elastic perfectly plastic model. The densification showed the creation of a pile up at the indenter face side that matches well with the experimental results.

Due to these discrepancies in the literature, it is of great interest to investigate the problem numerically in light of the material model verified in the previous section. FEA allows one to exclude any of the uncertainties related to frame compliance, tip geometry or iterative algorithms. The indenter surface is displaced to different depth (up to 180 nm) and the value of the contact area is calculated correspondingly assuming a known elastic modulus for the calibration material. Fig. 8 shows the numerical force curves obtained from the simulation.

The contact depth is calculated according to the Oliver Pharr fitting procedure [3] with no correction factors employed. The power

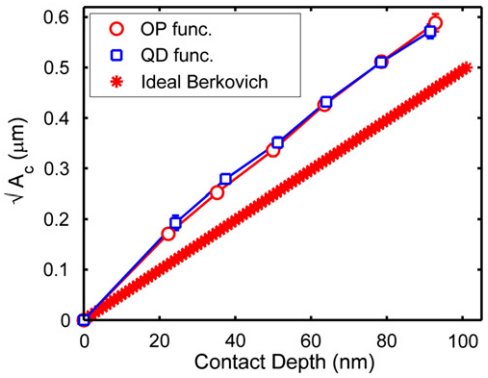

Fig. 7. Experimental tip area function for a Berkovich tip estimated using Oliver and Pharr (OP) method on fused silica (with no correction factors) compared to the ideal one. The material dependent method (OP power function and quadratic fitting function) significantly overestimated the tip area (The error bars are of one standard deviation).

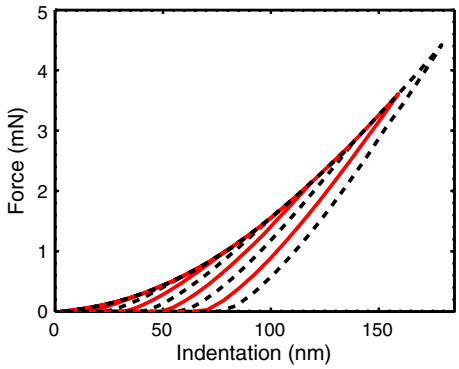

Fig. 8. Numerical force curves at different indentation depth utilized to obtain the tip area function.

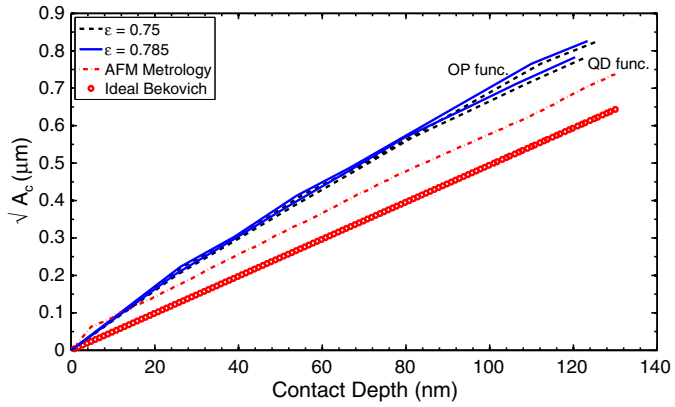

Fig. 9. Comparison between the tip metrology obtained by AFM and the tip area function obtained from the numerical force indentation curves. Oliver Pharr (OP) fitting function generated tip area that is higher than the quadratic function (QD). Using different ε values has minor effect on the estimated area. In general the estimated tip area is higher than the one obtained by AFM.

of the Oliver Pharr fitting function contributes to the value of ε and it generally has a value between 1.2 and 1.6 [3, 4, 38]. While ε has been found to change with depth, two values are generally used , 0.75 which is used by Oliver Pharr [3] and presented in ISO 14577–4, and 0.785 which was suggested by Martin and Troyon [2, 39] as an upper limit for the variation of ε with depth. Both values are used in calculating the contact depth in the present analysis to study their contribution to the estimated area function. The results are shown in Fig. 8.

The numerical findings are very similar to the ones obtained in the experimental results (see Fig. 7).The tip area obtained by AFM or estimated from force curves are both significantly larger than the idealized area of a Berkovich. The area obtained from fitting numerical force curves is found to be larger than the tip metrology from the AFM scan. The data from the AFM scan are believed to be more reliable due to the fact that it is independent of any iterative algorithms or frame compliance assumptions.

Fig. 9 proves that the calculated area is not an intensive property of the indenter but a convolution of the indenter topography by the fused silica deformation characteristics. Accordingly, it is noted that all the experiments performed by this calibration process are in reality referring the derived properties of any material to the deformation characteristics of fused silica [4]. Evidence of such outcome can be inferred from the work of Troyon and Huang [35] as they described the complex interaction between the correction factors utilized in estimating the elastic modulus. Although their reasoning was built upon the indenter tip deformation and tip blunting, their experimental findings on different materials provided contradictory results that do not support the argument. They concluded that the different elastic/plastic deformation of the materials during indentation can be the reason behind such discrepancies [35]. Shuman et al. [40] employed nanoindentation to study metals using a calibrated tip with fused silica. Apart from the influence of reverse plasticity demonstrated by metals, their estimated elastic modulus was consistently higher than the one obtained by tensile testing. Based on our findings, we believe that the fused silica calibration method contributed to such discrepancies when it comes to testing materials that have different deformation characteristics than fused silica.

The tip area deduced from AFM scans provides much of the information on the shape of the tip. It is seen that as the behavior of the square root of the contact area is not a straight line in contrast to the ideal tip shape (see Fig. 9) indicating that the geometry of the tip is affected by tip blunting and tip non-idealities at such shallow depths. This behavior was discussed earlier in [4, 31]. Fig. 9 points out that the quadratic fitting function of the unloading curve has a closer value to the AFM tip metrology than the Oliver Pharr power function when both function fitted the same section of the unloading curve (mid 80%). This was not clear in the experimental area function plots in Fig. 7 because the choice of the residual depth h_r in the OP function also plays a role in the calculations. Furthermore, studies showed that the value of the power of the Oliver Pharr function depends on the portion fitted from the unloading curve [34, 41], however, this kind of study is outside the scope of the current work. One can also observe that the value of ε does not have a significant effect on the obtained tip area in both fitting functions [3].

The values of the contact depth obtained from the fitting functions to the unloading section of the force indentation curves are summarized in Table 3 for two different values of ε. These values are compared to the contact depth obtained from FEA. Due to the complexity of the contact profile between the tip and the substrate in FEA, the contact depth is estimated by averaging the contact points' depth at the three sides of the tip.

It can be seen from the table that the value of power of the Oliver Pharr function lies between 1.4 and 1.6 which is higher than the values reported in the literature [1, 3, 4]. This can be caused by the portion fitted of the unloading curve and the value of residual depth utilized in the fitting as it is obtained exactly at zero load and not left as a fitting parameter. Comparing the calculated contact depth from FEA with the contact depths obtained from the Oliver Pharr function h_c (*OP*) and the quadratic fitting function h_c (*QD*), it is seen that the quadratic function showed closer agreement while the Oliver Pharr method consistently resulted in a higher contact depth. Again using different values of ε resulted in minor variation of about 2.5% in the contact depth.

In light of the obtained results, utilizing real tip geometry and an accurate material model, deeper understanding of the nanoindentation deformation process and material behavior and properties can be

Table 3
Contact depth values estimated from fitting the unloading curve of the numerical force curves with quadratic function or Oliver Pharr power function with two different ε values. (h_{max}: Maximum depth, h_r: Residual depth, h_c: Contact depth, QD: quadratic fitting, OP: Oliver Pharr fitting).

h_{max} (μm)	h_c (FEA) (μm)	Oliver Pharr (OP) fitting Parameters			ε = 0.75				ε = 0.785			
		m	a	h_r	hc (OP)	error%	hc (QD)	error%	hc (OP)	error%	hc (QD)	error%
0.04	0.0249	1.5839	0.0871	0.0117	0.0266	6.82	0.0253	1.60	0.0261	4.81	0.0247	−0.8
0.06	0.0376	1.45	0.0691	0.0213	0.0399	6.11	0.0392	4.25	0.039	3.72	0.0383	1.86
0.08	0.0511	1.5254	0.0984	0.0286	0.055	7.63	0.0533	4.3	0.0539	5.47	0.0521	1.95
0.1	0.0639	1.4248	0.0855	0.039	0.0681	6.57	0.0673	5.32	0.0666	4.22	0.0658	2.97
0.12	0.0767	1.5793	0.1332	0.0439	0.0847	10.43	0.0815	6.25	0.0831	8.34	0.0797	3.91
0.14	0.0901	1.4371	0.1046	0.0562	0.0969	7.54	0.0948	5.21	0.0949	5.32	0.0927	2.88
0.16	0.1035	1.4932	0.1232	0.0632	0.1122	8.4	0.1087	5.02	0.11	6.28	0.1063	2.7
0.18	0.1155	1.4232	0.1146	0.0755	0.1259	9	0.123	6.49	0.1234	6.83	0.1204	4.24

* Errors in h_c are calculated with respect to the value obtained from FEA.
**OP power function: $F = a(h\text{-}h_r)^m$.
***QD fitting function: $F = c_1h^2 + c_2h + c_3$.
**** $h_c = h_{max} - \varepsilon\,(F/S)$.

achieved. This can play a significant role in proposing new analytical approaches to enhance the accuracy of the nanoindentation experiments models. Tip imperfections have to be studied thoroughly to understand their effect on the obtained results especially at shallow indentation depth.

7. Conclusion

Deformation of fused silica is affected by the hydrostatic component of stress. We show that this deformation can be well described with the extended Drucker–Prager model which is available in commercial FEA packages. This model can be extended to study other amorphous materials with ease. The densification model results in a more realistic indent with a slight pile up at the face of the tip.

Area calibration of indenter tips produces an artificial area that takes into account fused silica properties and masks details of the tip itself. Using such an area in estimating other materials' properties which deform differently (metals or ceramics) may produce erroneous values.

Our numerical results show that the value of ε has minor effect on the estimated contact depth and can be used as a constant to simplify the analysis. Besides, the proposed framework and material model can assist studying ε in order to fill the gap on the area discrepancy. On the other hand, as the unloading fitting function is only used to get the slope of the unloading curve, a quadratic function can also be used to fit the curve.

Ultimately, AFM can be used to investigate the real tip geometry and can help in developing models that account for any tip imperfections without being affected by any assumptions related to tip geometry, frame compliance or iterative algorithms. Machine calibration standards could benefit from material-independent methods, as well as tip calibration standards.

References

[1] W. Oliver, G. Pharr, Improved technique for determining hardness and elastic modulus using load and displacement sensing indentation experiments, J. Mater. Res. 7 (6) (1992) 1564–1583.
[2] M. Martin, M. Troyon, Fundamental relations used in nanoindentation: Critical examination based on experimental measurements, J. Mater. Res. 17 (9) (2002) 2227–2234.
[3] W. Oliver, G. Pharr, Measurement of hardness and elastic modulus by instrumented indentation: advances in understanding and refinements to methodology, J. Mater. Res. 19 (3) (2004).
[4] T. Chudoba, N. Jennett, Higher accuracy analysis of instrumented indentation data obtained with pointed indenters, J. Phys. D: Appl. Phys. 41 (2008) 215407.
[5] K.R.Gadelrab, F.A. Bonilla, and M. Chiesa, *The Effect of Tip Rounding on Estimating the Elastic Modulus by means of Nanoindentation (Under Review). 2011.*
[6] A. Perriot, et al., Raman microspectroscopic characterization of amorphous silica plastic behavior, J. Am. Ceram. Soc. 89 (2) (2006) 596–601.
[7] G. Kermouche, et al., Mechanical modelling of indentation-induced densification in amorphous silica, Acta Mater. 56 (13) (2008) 3222–3228.
[8] M. Bertoldi, V. Sglavo, Soda-borosilicate glass: normal or anomalous behavior under Vickers indentation? J. Non-Cryst. Solids 344 (1–2) (2004) 51–59.
[9] B. Champagnon, et al., High pressure elastic and plastic deformations of silica: in situ diamond anvil cell Raman experiments, J. Non-Cryst. Solids 354 (2–9) (2008) 569–573.
[10] D. Vandembroucq, et al., Density hardening plasticity and mechanical ageing of silica glass under pressure: a Raman spectroscopic study, J. Phys. Condens. Matter 20 (2008) 485221.
[11] H. Ji, et al., Densification of window glass under very high pressure and its relevance to Vickers indentation, Scr. Mater. 55 (12) (2006) 1159–1162.
[12] K. Xin, J. Lambropoulos, Densification of fused silica: effects on nanoindentation, , 2000.
[13] T.H. Wang, T.-H. Fang, Y.-C. Lin, A numerical study of factors affecting the characterization of nanoindentation on silicon, Mater. Sci. Eng., A 447 (1–2) (2007) 244–253.
[14] T. Wang, T. Fang, Y. Lin, Analysis of the substrate effects of strain-hardening thin films on silicon under nanoindentation, Appl. Phys. A Mater. Sci. Process. 86 (3) (2007) 335–341.
[15] B. Poon, D. Rittel, G. Ravichandran, An analysis of nanoindentation in linearly elastic solids, Int. J. Solids Struct. 45 (24) (2008) 6018–6033.
[16] B. Poon, D. Rittel, G. Ravichandran, An analysis of nanoindentation in elasto-plastic solids, Int. J. Solids Struct. 45 (25–26) (2008) 6399–6415.
[17] S. Shim, W. Oliver, G. Pharr, A critical examination of the Berkovich vs. conical indentation based on 3D finite element calculation, , 2005.
[18] M. Lichinchi, et al., Simulation of Berkovich nanoindentation experiments on thin films using finite element method, Thin Solid films 312 (1–2) (1998) 240–248.
[19] F. Chen, R. Chang, Study of the effect of imperfect tips on nanoindentation by FEM, J. Mech. Sci. Technol. 21 (10) (2007) 1471–1476.
[20] M. VanLandingham, T. Juliano, M. Hagon, Measuring tip shape for instrumented indentation using atomic force microscopy, Meas. Sci. Technol. 16 (2005) 2173.
[21] Y. Kato, et al., Effect of densification on crack initiation under Vickers indentation test, J. Non-Cryst. Solids 356 (35-36) (2010) 1768–1773.
[22] J. Mackenzie, High pressure effects on oxide glasses: I, densification in rigid state, J. Am. Ceram. Soc. 46 (10) (1963) 461–470.
[23] S. Sakka, High pressure effects on glass, J. Non-Cryst. Solids 1 (1969) 107–142.
[24] Perriot, Nanoindentation de couches minces depose´es sur substrat de verre de silice, 2005.
[25] A. Khoei, Computational plasticity in powder forming processes, Elsevier Science Ltd, 2005.
[26] P. Kohnme, *ANSYS help documentation*, ANSYS, Inc. Theory Release, 2003, p. 8.
[27] W.G. Jiang, J.J. Su, X.Q. Feng, Effect of surface roughness on nanoindentation test of thin films, Eng. Fract. Mech. 75 (17) (2008) 4965–4972.
[28] M. Doerner, W. Nix, A method for interpreting the data from depth-sensing indentation instruments, J. Mater. Res. 1 (4) (1986) 601–609.
[29] K. Kese, M. Tehler, B. Bergman, Contact residual stress relaxation in soda-lime glass: Part I. Measurement using nanoindentation, J. Eur. Ceram. Soc. 26 (6) (2006) 1003–1011.
[30] J. Howell, J. Hellmann, C. Muhlstein, Correlations between free volume and pile-up behavior in nanoindentation reference glasses, Mater. Lett. 62 (14) (2008) 2140–2142.
[31] K. Herrmann, et al., Progress in determination of the area function of indenters used for nanoindentation, Thin Solid films 377 (2000) 394–400.
[32] J. Meneve, et al., Surface mechanical property testing by depth sensing indentation, Appl. Surf. Sci. 100 (1996) 64–68.
[33] K. Herrmann, et al., Characterisation of the geometry of indenters used for the micro-and nanoindentation method, Measurement 29 (3) (2001) 201–207.
[34] N. Jennett, J. Meneve, Depth sensing indentation of thin hard films: a study of modulus measurement sensitivity to indentation parameters, Mater. Res. Soc. Symp. Proc. 522 (1998) 239–244.
[35] M. Troyon, L. Huang, Correction factor for contact area in nanoindentation measurements, J. Mater. Res. 20 (3) (2005) 610–617.
[36] R. King, Elastic analysis of some punch problems for a layered medium, Int. J. Solids Struct. 23 (12) (1987) 1657–1664.
[37] J. Hay, A. Bolshakov, G. Pharr, A critical examination of the fundamental relations used in the analysis of nanoindentation data, J. Mater. Res. 14 (6) (1999) 2296–2305.
[38] A. Bolshakov, W. Oliver, G. Pharr, An explanation for the shape of nanoindentation unloading curves based on finite element simulation, Mater. Res. Soc. Symp. Proc. 356 (1995) 675–680.
[39] M. Troyon, M. Martin, A critical examination of the P–h relationship in nanoindentation, Appl. Phys. Lett. 83 (2003) 863.
[40] D.J. Shuman, A.L.M. Costa, M.S. Andrade, Calculating the elastic modulus from nanoindentation and microindentation reload curves, Mater. Charact. 58 (4) (2007) 380–389.
[41] G. Kaupp, *Nanoindentation*, in *Atomic Force Microscopy, Scanning Nearfield Optical Microscopy and Nanoscratching*, Springer, Berlin Heidelberg, 2006, pp. 177–227.